Identifiability of location and magnitude of flow barriers in slightly compressible flow

Kahrobaei, S.; Mansoori Habibabadi, M.; Joosten, G. J P; Van Den Hof, P. M J; Jansen, J. D.

DOI
10.2118/173235-PA

Publication date
2016

Document Version
Final published version

Published in
SPE Journal

Identifiability of Location and Magnitude of Flow Barriers in Slightly Compressible Flow

S. Kahrobaei, Delft University of Technology; **M. Mansoori Habibabadi,** Delft University of Technology and Sharif University of Technology; **G. J. P. Joosten,** Shell Global Solutions International, **P. M. J. Van den Hof,** Eindhoven University of Technology; and **J. D. Jansen,** Delft University of Technology

Summary

Classic identifiability analysis of flow barriers in incompressible single-phase flow reveals that it is not possible to identify the location and permeability of low-permeability barriers from production data (wellbore pressures and rates), and that only averaged reservoir properties in between wells can be identified. We extend the classic analysis by including compressibility effects. We use two approaches: a twin experiment with synthetic production data for use with a time-domain parameter-estimation technique, and a transfer-function formalism in the form of bilaterally coupled four-ports allowing for an analysis in the frequency domain. We investigate the identifiability, from noisy production data, of the location and the magnitude of a low-permeability barrier to slightly compressible flow in a 1D configuration. We use an unregularized adjoint-based optimization scheme for the numerical time-domain estimation, by use of various levels of sensor noise, and confirm the results by use of the semianalytical transfer-function approach. Both the numerical and semianalytical results show that it is possible to identify the location and the magnitude of the permeability in the barrier from noise-free data. By introducing increasingly higher noise levels, the identifiability gradually deteriorates, but the location of the barrier remains identifiable for much-higher noise levels than the permeability. The shape of the objective-function surface, in normalized variables, indeed indicates a much-higher sensitivity of the well data to the location of the barrier than to its magnitude. These theoretical results appear to support the empirical finding that unregularized gradient-based history matching in large reservoir models, which is well-known to be a severely ill-posed problem, occasionally leads to useful results in the form of model-parameter updates with unrealistic magnitudes but indicating the correct location of model deficiencies.

Introduction

Estimating reservoir parameters from measured data is an ill-posed inverse problem because of the large number of parameters and the limited available data (Shah et al. 1978; Oliver et al. 2008). Consequently, it is important to understand which parameters can be estimated with reasonable accuracy from the available data. This aspect can be addressed as determining the identifiability of the parameters.

From a systems-and-control-theory perspective, the transient response of a dynamic system contains information about dynamics-related properties of a system. Consequently, including compressibility effects (leading to a transient response) can result in a more-accurate reservoir-parameter estimation than just considering the steady-state response. The pressure behavior of a slightly compressible single-phase fluid in a reservoir can be described accurately by the diffusivity equation. Theoretically, the transient-pressure response of every point in a reservoir to a step or impulse input may contain information about reservoir boundaries and reservoir heterogeneities (Grader and Horne 1988; Van Doren 2010). However, certain parameters have a more-significant effect on this transient response than others, and in many cases a unique identification of parameters is not possible. Subsequently, by investigating the effect of different parameters on the dynamic behavior, we can understand which parameters are more identifiable from the available data. On the other hand, presence of noise in the data may hamper the identifiability of such parameters and can result in unrealistic parameter estimates (Dogru et al. 1977). Hence, it is important to also investigate the effect of noise on identifiability of different parameters.

Identifiability of reservoir heterogeneity has been studied by many authors both from a classic well-testing perspective and from a systems-and-control perspective (Stallman 1952; Watson et al. 1984; Yaxley 1987; Grader and Horne 1988; Feitosa et al. 1994; Oliver 1996; Van Doren et al. 2008; Zandvliet et al. 2008; Ahn and Horne 2010; Van Doren 2010). The concept of identifiability as used in systems-and-control theory can loosely be defined as the capacity to infer the magnitude of model parameters from given specific input and output data. Moreover, the concept of structural identifiability is, loosely speaking, concerned with whether it is possible to infer the magnitude of model parameters at all from input/output data, assuming an optimally chosen, "persistently exciting" input. Van Doren (2010) provides a more-precise, mathematical definition of (structural) identifiability as applied to porous-media flow. Stallman (1952) analyzed the pressure response of a constant-rate well and presented log/log-type curves for constant-pressure boundaries as well as impermeable linear boundaries. Watson et al. (1984) investigated the identifiability of estimates of two-phase reservoir properties in history matching. They concluded that for single-phase incompressible flow, only the harmonic average of the permeability distribution is identifiable, and subsequently the presence of the saturation distribution is essential to identify the absolute-permeability spatial distribution. Yaxley (1987) investigated the effects of a partially communicating linear fault on transient-pressure behavior. Grader and Horne (1988) and Ahn and Horne (2010) considered (slightly) compressible flow and used well-testing-related methods such as interference testing and pulse testing to investigate the detectability of reservoir heterogeneities. They showed that there is sometimes information about the distance between wells and flow-relevant features (e.g., reservoir boundaries, impermeable subregions, or permeability distribution) in the data, although to a limited extent because of the diffusive nature of pressure transients.

The objective of this study is to investigate the identifiability of location and magnitude of a flow barrier in compressible single-phase flow by analyzing the effect of this heterogeneity on dynamical behavior of the flow. The motivation stems from a study by Joosten et al. (2011) that showed that sometimes the application of unregularized reservoir-parameter estimation still appears to have added value. They argued, by use of numerical examples, that localized unrealistic-parameter values can be used as an indicator of model errors in the underlying reservoir model, a concept that they named "model maturation." In a follow-up study,

This paper (SPE 173235) was accepted for presentation at the SPE Reservoir Simulation Symposium, Houston, 23–25 February 2015, and revised for publication. Original manuscript received for review 9 June 2015. Revised manuscript received for review 19 August 2015. Paper peer approved 24 August 2015.

Fig. 1—Permeability field of a 1D homogeneous reservoir model with a low-permeability barrier. Permeability values are expressed as the natural logarithm of permeability in md. The blue and orange dots indicate the injector and the producer, respectively.

Fig. 2—Permeability field of the starting model. Permeability values are expressed as the natural logarithm of permeability in md. The blue and orange dots indicate the injector and the producer, respectively.

Kahrobaei et al. (2014) showed that the application of unregularized reservoir-parameter estimation may sometimes give an indication of the location of significant missing features in the model. In the present study we further analyze this phenomenon by addressing the identifiability of flow-relevant features. In particular, we apply two approaches to study the possibility of detecting a low-permeability barrier from the observations (outputs of the system). In the first approach, we conduct three different twin-experiments with synthetic production data contaminated with different noise levels in the time domain. In our twin experiments, an unregularized parameter estimation is applied to update uncertain parameters (gridblock permeabilities) in a 1D reservoir model that contains a major deficiency in the form of a missing low-permeability feature. In the second approach, we develop an analytical method to explain our time-domain findings. In this approach we consider flow through porous media as a linear system and develop a method that gives an analytical expression for the dynamic characteristics of the system as a function of the system's geometric properties and heterogeneity in the frequency domain. This solution is obtained by use of a transfer-function formalism applied to a series of bilaterally coupled porous-media models.

The structure of this study is as follows: Next we present and discuss the numerical twin-experiment results in the time domain. The transfer-function formulation is derived next. Afterward we investigate effects of location and magnitude of a flow barrier on the output of a system and present and discuss the parameter-estimation results on the basis of the frequency responses of the system. Next, the objective-function space is visualized and the (structural) parameter identifiability is discussed. We end the study with a brief discussion and conclusions.

Time-Domain Twin Experiments

We perform three twin experiments. They all use the same "truth model" to generate synthetic data, but the resulting data are contaminated with different noise levels. The first experiment involves the assimilation of noise-free production data, whereas in the last two experiments we assimilate noisy production data.

Synthetic Truth. Consider 1D single-phase flow of a slightly compressible fluid through a porous medium. The domain has a homogeneous permeability distribution with a low-permeability barrier in between. The size of the reservoir is $500\times50\times2$ m, which is divided into 50 gridblocks. Fluid compressibility is 1.0×10^{-7} Pa^{-1}, and fluid viscosity is 1×10^{-3} Pa·s. The reservoir is produced with an injector at the left side and a producer at the right side. A low-permeability barrier with a width of 30 m is located 350 m from the injector. The background permeability is 300 md, and the permeability of the barrier is 0.1 md. The reservoir has a uniform porosity of 0.2. The initial pressure is 300 MPa. The producer is operating at a bottomhole pressure of 250 MPa and the injector at a constant flow rate of 0.002 m^3/s (172.8 m^3/d). The reservoir is simulated for 1,000 days and we measure the flow rates in the producer on a daily basis. **Fig. 1** shows the permeability field of the reservoir with its low-permeability barrier.

Starting Reservoir Model. The low-permeability barrier in the reservoir is missing in the starting model. All remaining parameters in the starting model are identical to those of the truth case. **Fig. 2** depicts the uniform-permeability field of the starting model with a constant permeability of 300 md.

For parameter-estimation purposes we try to minimize an objective function, which is defined as a mismatch between observed data and simulated data:

$$J(\mathbf{m}) = [\mathbf{d} - \mathbf{y}(\mathbf{m})]^T \mathbf{P}_d^{-1} [\mathbf{d} - \mathbf{y}(\mathbf{m})], \quad \ldots\ldots\ldots\ldots\ldots (1)$$

where $\mathbf{m}$ is a vector of unknown model parameters (gridblock permeabilities for the present study), $\mathbf{d}$ is a vector of data (measurements), $\mathbf{y}$ is a vector-valued function that relates the model parameters to the model outputs (i.e., the simulated data), and $\mathbf{P}_d$ is a square positive semidefinite matrix of weight factors that is chosen as the measurement-error covariance matrix. Minimization of the objective function is achieved by adjustment of the model parameters $\mathbf{m}$. Various numerical techniques are available to perform this minimization, with the most-efficient one being gradient-based minimization where the gradient is computed by use of the adjoint method (Oliver et al. 2008). For the present study, we used an in-house reservoir simulator with adjoint functionality to calculate the gradients of the objective function (Kraaijevanger et al. 2007). We used the limited-memory Broyden-Fletcher-Goldfarb-Shanno method to minimize the objective function (Gao and Reynolds 2006).

Experiment No. 1: Parameter Estimation on the Basis of Noise-Free Measurements. In the first twin experiment, parameter estimation is performed starting from the uniform reservoir model, depicted in Fig. 2, on the basis of the perfect (noise-free) production data. **Fig. 3** shows the updated permeability field after parameter estimation. For this experiment, the covariance matrix is chosen as an identity matrix.

Fig. 3—Updated permeability field of the 1D reservoir model for Experiment No. 1. Permeability values are expressed as the natural logarithm of permeability in md.

Model	Gridblock No.	Permeability value (md)
Truth parameters	36	0.1
	37	0.1
	38	0.1
Updated parameters	36	0.1
	37	0.0997
	38	0.1

Table 1—Gridblock numbers and permeabilities of the low-permeability barrier in the truth and the updated models.

Table 1 lists the gridblock numbers and corresponding permeability values of the low-permeability barrier in the truth case and the updated model (Figs. 1 and 3, respectively).

As can be seen in Table 1, the gridblock numbers and the gridblock permeabilities of the low-permeability barrier in the updated model are exactly the same as those in the truth case.

Experiment No. 2: Parameter Estimation on the Basis of Noisy Measurements: High Signal/Noise Ratio. In second twin experiment, parameter estimation is performed starting from the same reservoir model as Experiment No. 1 but on the basis of noisy production data. Errors are generated by sampling from a Gaussian distribution with zero mean and a standard deviation equal to 27.8×10^{-3} m^3/s (1 m^3/d). Negative production rates, after the addition of noise, are reset to zero. It is assumed that the measurements were affected by independent noise, which results in a diagonal covariance matrix with equal-magnitude elements for the observation errors. The same covariance matrix was used in the objective function defined by Eq. 1. **Fig. 4** depicts the updated permeability field after parameter estimation on the basis of noisy data (with known covariance).

Table 2 lists the gridblock numbers and corresponding permeability values of the low-permeability barrier in the truth case and the updated model for Experiment No. 2.

As can be seen in Table 2, in the experiment with noisy measurements the positions of the low-permeability barriers in the truth case and the updated model are exactly the same, but the permeability value of the corresponding gridblocks in the updated model are not as accurate as those obtained in the noise-free experiment.

Experiment No. 3: Parameter Estimation on the Basis of Noisy Measurements: Low Signal/Noise Ratio. In the third twin experiment, the amount of error in the data is increased in comparison with Experiment No. 2. In this case, the errors are generated from a Gaussian distribution with zero mean and a standard deviation equal to 278×10^{-3} m^3/s (10 m^3/d) by use of the same approach as in the previous experiment. **Fig. 5** depicts the updated permeability field of the 1D reservoir model after parameter estimation.

Table 3 lists the gridblock numbers and corresponding permeability values of the low-permeability barrier in the truth case and the updated model for Experiment No. 3.

As can be seen in Table 3, by increasing the noise level in the measurements, the positions of the gridblocks with the lowest permeabilities in the updated model and the truth case are still identical, but the permeability values of those gridblocks are now significantly different. The harmonic average over all gridblocks on the basis of true permeability distribution is 1.65, and for the noise-free experiment, the low-level-noise experiment, and the high-level-noise experiment they are 1.65, 1.66, and 1.30, respectively.

We note that the deviation of our estimates from the true values is caused by random noise in the measurements. Different realizations of the measurement noise will therefore result in different deviations of the estimates.

Transfer-Function Representation

To further analyze the behavior that was observed in our 1D twin experiments in the time domain, we conduct 1D experiments by use of a transfer-function formalism to characterize the identifiability of the location and magnitude of model deficiencies (absence of flow barriers). We use a two-port network approach that results in a lumped-parameter representation of our system (Carslaw and Jaeger 1959). The structure of the 1D initial-boundary-value problem allows for the input/output representation of the system in terms of pressure and flow rate at two points in the spatial domain, mapped by a linear transformation.

Model Description. The 1D reservoir model that was described previously can be considered as a system that consists of three blocks. The total length of the domain and the length of the middle block are known. The length of the first block of the domain is unknown, resulting in an unknown position of the middle block. Note that length of the third block is a function of the length of the first block because the total length of the domain is constant. The middle block works as a barrier to flow from Point 1 to Point 4 **(Fig. 6).**

Governing Equations. The pressure behavior of a slightly compressible single-phase fluid in a reservoir can be described by the diffusivity equation. The pressure-diffusion equation for linear flow between two points can be written as

$$\frac{\partial p(x,t)}{\partial t}=\eta\frac{\partial^2 p(x,t)}{\partial x^2}, \quad \ldots\ldots\ldots\ldots\ldots\ldots\ldots\ldots\ldots (2)$$

in which η is defined as hydraulic diffusivity,

$$\eta=\frac{k}{\phi\mu c_t}, \quad \ldots\ldots\ldots\ldots\ldots\ldots\ldots\ldots\ldots\ldots\ldots (3)$$

where k is permeability, ϕ is porosity, μ is viscosity, and c_t is total compressibility. Moreover, the flow rate for linear flow can be written as

$$q(x,t)=-A\frac{k}{\mu}\frac{\partial p(x,t)}{\partial x}, \quad \ldots\ldots\ldots\ldots\ldots\ldots\ldots\ldots\ldots (4)$$

where A is the surface area.

Note that wells in Fig. 6 are to be imagined as (infinite conductivity) fractures fully penetrating a channel of constant cross section A, and that skin, wellbore storage, and near-well radial-flow convergence are neglected.

Dimensionless Variables. To transform Eqs. 2 and 4 into dimensionless equations, various dimensionless variables are defined.

Dimensionless length is defined as

$$\xi=\frac{x}{L}, \quad \ldots\ldots\ldots\ldots\ldots\ldots\ldots\ldots\ldots\ldots\ldots\ldots\ldots (5)$$

Fig. 4—Updated permeability field of the 1D reservoir model for Experiment No. 2. Permeability values are expressed as the natural logarithm of permeability in md.

Model	Gridblock No.	Permeability value (md)
Truth parameters	36	0.1
	37	0.1
	38	0.1
Updated parameters	36	0.1036
	37	0.1206
	38	0.08

Table 2—Gridblock numbers and permeabilities of the low-permeability barrier in the truth and the updated models.

where L is total constant length of the first and the last blocks of Fig. 6.

Dimensionless pressure is defined as

$$\pi = \frac{p - p_i}{\hat{p}}, \quad (6)$$

where $\hat{p}$ is the pressure at the outlet boundary and p_i is initial pressure.

Dimensionless time is defined as

$$\tau = \frac{kt}{\mu c_t \phi L^2}. \quad (7)$$

By use of these dimensionless variables, we can rewrite Eqs. 2 and 4 in dimensionless form:

$$\frac{\partial \pi}{\partial \tau} = \frac{\partial^2 \pi}{\partial \xi^2}, \quad (8)$$

$$\theta = -\alpha \frac{\partial \pi}{\partial \xi}, \quad (9)$$

where θ is dimensionless flow rate defined as

$$\theta = \frac{q}{\hat{q}}, \quad (10)$$

and α is a dimensionless number defined as

$$\alpha = \frac{Ak\hat{p}}{L\mu\hat{q}}, \quad (11)$$

in which $\hat{q}$ is the flow rate at the inlet boundary.

In this study, Eqs. 8 and 9 will be applied in three different regions of constant permeability.

Transfer-Function Derivation. To find input/output relations of the system depicted in Fig. 6, first the transfer functions of each block are derived and then they are coupled together to obtain transfer functions that describe the entire system. In the next subsection we derive the transfer functions for the first block of the system depicted in Fig. 6. Similar derivations would apply to the other blocks as well.

Input/Output Relations of One Block of the System. By applying a Laplace transform to Eq. 8, we obtain

$$\frac{\partial^2}{\partial \xi^2}\Pi(\xi, s) - s\Pi(\xi, s) = 0. \quad (12)$$

Eq. 12 has a solution of the form

$$\Pi(\xi, s) = C_1 e^{\xi\sqrt{s}} + C_2 e^{-\xi\sqrt{s}}. \quad (13)$$

Moreover, Eq. 9 can also be written in the Laplace domain as follows:

$$\Theta(\xi, s) = -\alpha C_1 \sqrt{s} e^{\xi\sqrt{s}} + \alpha C_2 \sqrt{s} e^{-\xi\sqrt{s}}, \quad (14)$$

where functions C_1 and C_2 can be determined by requiring the solution to satisfy the boundary conditions that are chosen as flow rate at the left side and pressure at the right side of the block; that is, $\Theta(\xi, s) = \Theta(\xi_1, s)$ at $\xi = \xi_1$ and $\Pi(\xi, s) = \Pi(\xi_2, s)$ at $\xi = \xi_2$. Consequently, solving for C_1 and C_2 leads to

$$C_1 = \frac{1}{\Lambda(s) + \Lambda^{-1}(s)}\Pi(\xi_2, s) - \frac{1}{\alpha\sqrt{s}}\frac{\Lambda^{-1}(s)}{\Lambda(s) + \Lambda^{-1}(s)}\Theta(\xi_1, s), \quad (15)$$

$$C_2 = \frac{1}{\Lambda(s) + \Lambda^{-1}(s)}\Pi(\xi_2, s) + \frac{1}{\alpha\sqrt{s}}\frac{\Lambda(s)}{\Lambda(s) + \Lambda^{-1}(s)}\Theta(\xi_1, s), \quad (16)$$

in which

$$\Lambda(s) = e^{\xi_2\sqrt{s}}. \quad (17)$$

At the boundaries we have the following output variables:

$$\Pi(\xi_1, s) = C_1 + C_2, \quad (18)$$

$$\Theta(\xi_2, s) = -\alpha C_1 \sqrt{s}\Lambda(s) + \alpha C_2 \sqrt{s}\Lambda^{-1}(s). \quad (19)$$

Inserting values of C_1 and C_2 from Eqs. 15 and 16 into Eqs. 18 and 19 gives the final solutions:

$$\Pi(\xi_1, s) = \frac{2}{\Lambda(s) + \Lambda^{-1}(s)}\Pi(\xi_2, s) + \frac{1}{\alpha\sqrt{s}}\frac{\Lambda(s) - \Lambda^{-1}(s)}{\Lambda(s) + \Lambda^{-1}(s)}\Theta(\xi_1, s), \quad (20)$$

$$\Theta(\xi_2, s) = \alpha\sqrt{s}\frac{\Lambda^{-1}(s) - \Lambda(s)}{\Lambda(s) + \Lambda^{-1}(s)}\Pi(\xi_2, s) + \frac{2}{\Lambda(s) + \Lambda^{-1}(s)}\Theta(\xi_1, s). \quad (21)$$

Subsequently, $\Theta(\xi_2, s)$ and $\Pi(\xi_1, s)$ can be written as a function of the boundary conditions:

$$\begin{bmatrix}\Theta(\xi_2, s)\\ \Pi(\xi_1, s)\end{bmatrix} = \begin{bmatrix}A_{11} & A_{12}\\ A_{21} & A_{22}\end{bmatrix}\begin{bmatrix}\Theta(\xi_1, s)\\ \Pi(\xi_2, s)\end{bmatrix}, \quad (22)$$

where A_{ij} are the transfer functions of the first block, which explain the input/output relations as a function of model parameters. These transfer functions can be derived as

$$A_{11} = \frac{2}{e^{\xi_2\sqrt{s}} + e^{-\xi_2\sqrt{s}}} = \frac{1}{\cosh(\xi_2\sqrt{s})}, \quad (23)$$

$$A_{12} = \alpha\sqrt{s}\frac{e^{-\xi_2\sqrt{s}} - e^{\xi_2\sqrt{s}}}{e^{\xi_2\sqrt{s}} + e^{-\xi_2\sqrt{s}}} = -\alpha\sqrt{s}\tanh(\xi_2\sqrt{s}), \quad (24)$$

$$A_{21} = \frac{1}{\alpha\sqrt{s}}\frac{e^{\xi_2\sqrt{s}} - e^{-\xi_2\sqrt{s}}}{e^{\xi_2\sqrt{s}} + e^{-\xi_2\sqrt{s}}} = \frac{1}{\alpha\sqrt{s}}\tanh(\xi_2\sqrt{s}), \quad (25)$$

Fig. 5—Updated permeability field of the 1D reservoir model for Experiment No. 3. Permeability values are expressed as the natural logarithm of permeability in md.

Model	Gridblock No.	Permeability value (md)
Truth parameters	36	0.1
	37	0.1
	38	0.1
Updated parameters	36	0.026
	37	19.15
	38	89.6

Table 3—Gridblock numbers and permeabilities of the low-permeability barrier in the truth and the updated models.

$$A_{22} = \frac{2}{e^{\xi_2\sqrt{s}} + e^{-\xi_2\sqrt{s}}} = \frac{1}{\cosh(\xi_2\sqrt{s})}. \quad \ldots\ldots\ldots\ldots (26)$$

In this way we can derive the transfer functions for each block of our system.

Input/Output Relations of the Entire System. By coupling the transfer functions of the three blocks, we can derive the input/output relations for the entire system. **Fig. 7** depicts the coupled model in block-diagram representation for our 1D reservoir model, where we used the letters A, B, and C to indicate the three consecutive blocks of Fig. 6.

Each block of Fig. 7 has an input/output relation in the form of Eq. 22. Consequently, by performing matrix multiplications, we can find the transfer functions that represent the input/output relations for the entire system. The matrix form of the input/output relations can be written as

$$\begin{bmatrix} \Theta(\xi_4, s) \\ \Pi(\xi_1, s) \end{bmatrix} = \begin{bmatrix} S_{11} & S_{12} \\ S_{21} & S_{22} \end{bmatrix} \begin{bmatrix} \Theta(\xi_1, s) \\ \Pi(\xi_4, s) \end{bmatrix}, \quad \ldots\ldots\ldots\ldots (27)$$

where the elements S_{ij} are given by

$$S_{11} = -\frac{A_{11}B_{11}C_{11}}{C_{21}(B_{12} + A_{12}B_{11}B_{22} - A_{12}B_{12}B_{21}) + A_{12}B_{21} - 1}, \quad \ldots\ldots\ldots\ldots (28)$$

$$S_{12} = -\frac{\begin{array}{c} C_{12} - A_{12}C_{12}B_{21} + C_{11}C_{22}B_{12} - C_{12}C_{21}B_{12} \\ + A_{12}C_{11}C_{22}B_{11}B_{22} - A_{12}C_{11}C_{22}B_{12}B_{21} \\ - A_{12}C_{12}C_{21}B_{11}B_{22} + A_{12}C_{12}C_{21}B_{12}B_{21} \end{array}}{A_{12}B_{21} + C_{21}B_{12} + A_{12}C_{21}B_{11}B_{22} - A_{12}C_{21}B_{12}B_{21} - 1}, \quad \ldots\ldots\ldots\ldots (29)$$

$$S_{21} = -\frac{\begin{array}{c} A_{21} + A_{11}A_{22}B_{21} - A_{12}A_{21}B_{21} - A_{21}C_{21}B_{12} \\ + A_{11}A_{22}C_{21}B_{11}B_{22} - A_{11}A_{22}C_{21}B_{12}B_{21} \\ - A_{12}A_{21}C_{21}B_{11}B_{22} + A_{12}A_{21}C_{21}B_{12}B_{21} \end{array}}{A_{12}B_{21} + C_{21}B_{12} + A_{12}C_{21}B_{11}B_{22} - A_{12}C_{21}B_{12}B_{21} - 1}, \quad \ldots\ldots\ldots\ldots (30)$$

$$S_{22} = -\frac{A_{22}C_{22}B_{22}}{A_{12}(B_{21} + C_{21}B_{11}B_{22} - C_{21}B_{12}B_{21}) + C_{21}B_{12} - 1}, \quad \ldots\ldots\ldots\ldots (31)$$

where A_{ij}, B_{ij}, and C_{ij} are the transfer functions of the three consecutive blocks of Fig. 6. Consequently, the block diagram of the system (Fig. 7) can be simplified to the configuration depicted in **Fig. 8.**

Effect of Location and Magnitude of Barrier on Dynamic System Output

In the time-domain twin experiments, we used flow rates in the injector and pressures in the producer as inputs and flow rates in the producer as outputs. Therefore, we can simplify the configuration depicted in Fig. 8 in such a way that the single output of our system, $\Theta(\xi_4, s)$, is influenced by two inputs: $\Theta(\xi_1, s)$ and $\Pi(\xi_4, s)$. Consequently, the input/output relation of the system is described by the transfer functions S_{11} and S_{12} only **(Fig. 9).**

With the aid of Eq. 27, we can now write an expression for the system output:

$$\Theta(\xi_4, s) = \Theta(\xi_1, s)S_{11} + \Pi(\xi_4, s)S_{12}. \quad \ldots\ldots\ldots\ldots (32)$$

Because we used step inputs in the time-domain twin experiments, the dimensionless form of our inputs in the Laplace domain can be written as

$$\Theta(\xi_1, s) = \frac{1}{s}, \quad \ldots\ldots\ldots\ldots (33)$$

$$\Pi(\xi_4, s) = \frac{1}{s}. \quad \ldots\ldots\ldots\ldots (34)$$

By substituting Eqs. 33 and 34 into Eq. 32, the output of the system can be written as

$$\Theta_{\text{out}} = \Theta(\xi_4, s) = \frac{1}{s}S_{11} + \frac{1}{s}S_{12} = \frac{1}{s}(S_{11} + S_{12}). \quad \ldots\ldots (35)$$

Note that all the variables, and therefore the transfer functions, are dimensionless.

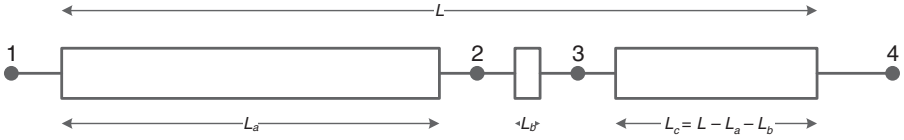

Fig. 6—Schematic of two 1D domains separated by a low-permeability barrier.

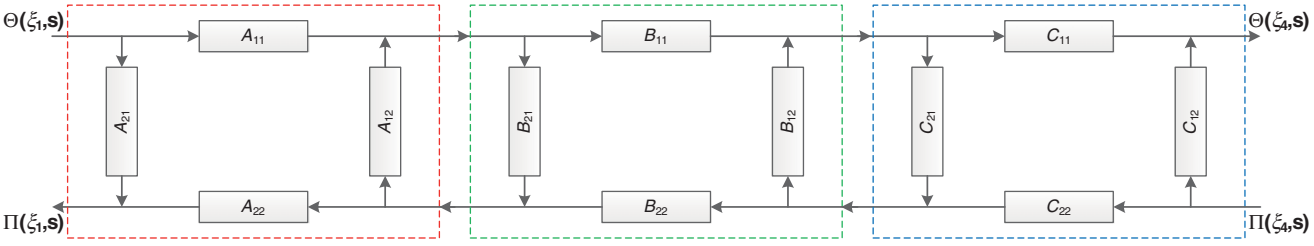

Fig. 7—Coupled model in block-diagram representation for the model depicted in Fig. 6.

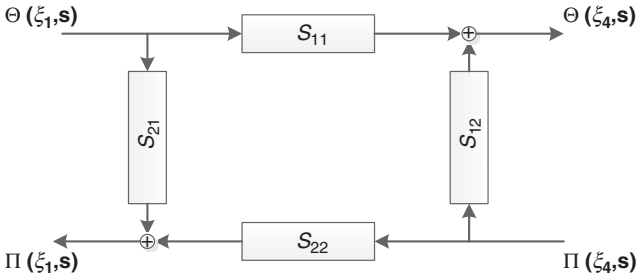

Fig. 8—Modified block-diagram representation for the model depicted in Fig. 6.

Parameters	Magnitude	Unit
$L_a/L=\xi_2-\xi_1$	0.7	–
$L_b/L=\xi_3-\xi_2$	0.06	–
α_a, α_c	0.75	–
α_b	0.0025	–

Table 4—Truth parameter values.

At this stage we can replace s in Eq. 35 with $j\omega_D$, where j is the imaginary unit and ω_D is dimensionless frequency. Dimensionless sampling frequency is defined according to sampling dimensionless time in our time-domain experiments. This will result in a frequency-response description of our system. Now we are able to investigate the effect of location and magnitude of the middle block (the flow barrier) on the output of our system. To perform a sensitivity analysis and a parameter estimation, which are presented later in the study, we define a "truth" case, with parameters listed in **Table 4.** The truth parameters are equivalent to the parameters of the time-domain truth case. Moreover, in our experiments the dimensionless frequency range is chosen between 0.6 and 600. The analytical truth case is used to generate synthetic measurements for parameter-estimation purposes in the later section Parameter Estimation in the Frequency Domain.

Effect of Location of a Flow Barrier. In this case we vary the location (ξ_2) of the middle block of the system, whereas the permeability magnitude of that block is fixed at a small value ($\alpha_b = 0.0025$), and evaluate the corresponding output of the system by use of Eq. 35. **Fig. 10** depicts the amplitude of the system output for different middle-block positions at different frequencies. The dashed line in Fig. 10 is the amplitude of the system output in the absence of the flow barrier.

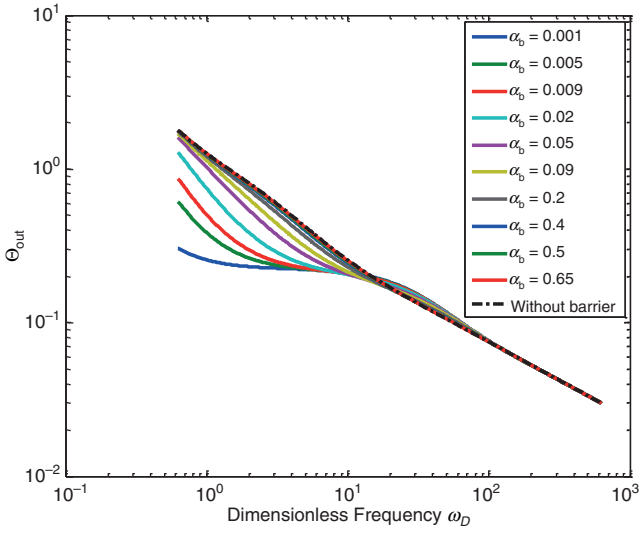

Fig. 11—Amplitude of system output for different barrier-permeability magnitude and fixed location.

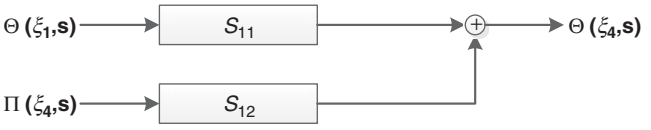

Fig. 9—Input/output relation in the reservoir system.

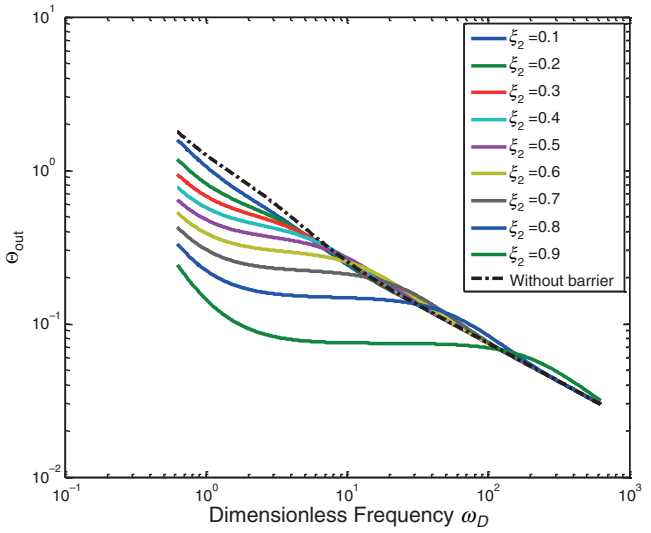

Fig. 10—Amplitude of system output for different barrier position and a fixed low-barrier-permeability magnitude.

As can be seen in Fig. 10, the output of the system is quite sensitive to the location of the middle block when it has a small magnitude. In the other words, the location of the low-permeability barrier significantly affects the output of our system. Moreover, it can be concluded from Fig. 10 that when the barrier location is closer to the producer, it has more effect on the output.

Effect of Permeability Magnitude of a Flow Barrier. In this case we vary the permeability magnitude (α_b) of the middle block of the system while its location is fixed ($\xi_2 = 0.7$). Subsequently we evaluate the corresponding output of the system for different values of the middle block's permeability magnitude. **Fig. 11** depicts the frequency response for these cases. Dashed line in Fig. 11 is the amplitude of the system output in the absence of the flow barrier.

It can be clearly seen that as the permeability magnitude of the middle block increases—that is, as the resistance to flow decreases—the output of the system becomes less sensitive to the magnitude variations.

Parameter Estimation in the Frequency Domain

In this section we try to estimate uncertain parameters by use of frequency responses obtained from the transfer function of the system. In this study the location (ξ_2) and magnitude (α_b) of the middle block are considered as unknown parameters (Fig. 6). We try to estimate these parameters by minimizing a mismatch objective function defined as

$$V = (\Theta_{obs} - \Theta_{out})^T \mathbf{P}_\Theta^{-1} (\Theta_{obs} - \Theta_{out}), \quad \ldots\ldots\ldots\ldots \quad (36)$$

where Θ_{obs} is the truth output vector, which is generated by use of truth parameters and Eq. 35 at different frequencies by replacing s with $j\omega$. Vector Θ_{out} is the simulated output. The starting model parameters are identical to the truth parameters except for the middle-block location and magnitude. $\mathbf{P}_\Theta$ is the measurement-

Parameters	Truth Value	Starting Value	Estimated Value
ξ_2	0.7	0.4	0.7
α_b	0.0025	0.75	0.0025

Table 5—Model parameters for Experiment No. 1.

Parameters	Truth Value	Starting Value	Estimated Value
ξ_2	0.7	0.4	0.69
α_b	0.0025	0.75	0.0026

Table 6—Model parameters for Experiment No. 2.

error covariance matrix, which is chosen as an identity matrix in this study. Note that the derivative of the objective function can be calculated analytically. Moreover, because the data vectors (observed and model output) consist of complex numbers, we can make our data real-valued by considering them as 2D data points; i.e., with real and imaginary parts (Blom and Van den Hof 2010). Following this approach, we define an augmented-data vector by stacking the real and imaginary parts of the complex-valued vectors.

Experiment No. 1: Noise-Free Parameter Estimation. In the first experiment we use noise-free measurements for parameter-estimation purposes. Eq. 36 is minimized by adjustment of the location and the magnitude of the middle block. The minimization converges in 15 iterations. The truth-, starting-, and estimated-parameter values for this experiment are listed in **Table 5.**

It can be concluded from Table 5, similar to Experiment No. 1 in time domain, that in the case of noise-free measurements we are able to retrieve the location and the magnitude of a low-permeability barrier with 100% accuracy.

Noise Effect on Estimation of Location and Magnitude of a Low-Permeability Barrier. In presence of noise, Eq. 35 can be written as

$$\Theta_{\text{out}} = \frac{1}{j\omega}(S_{11} + S_{12}) + \nu, \quad \ldots\ldots\ldots\ldots\ldots\ldots \quad (37)$$

where ν represents Laplace-transformed noise converted to the frequency domain. If we assume to have Gaussian white noise in the time domain, which is the case in our time-domain examples, this transformation also results in white noise in the frequency domain. Note that in our experiments noise only affects the output.

Experiment No. 2: High Signal/Noise Ratio. In this experiment, we generate white noise from the same distribution as used in the subsection Experiment No. 2: Parameter Estimation Based on Noisy Measurements: High Signal/Noise Ratio for the high signal/noise-ratio experiment in the time domain, and use a Fourier transform to transform the noise to the frequency domain. Subsequently, we perform parameter estimation on the basis of this noisy data. The minimization converges in 14 iterations. The truth-, starting-, and estimated-parameter values for this experiment are listed in **Table 6.**

It can be concluded from Table 6, similar to Experiment No. 2 in the time domain, that for a low amount of noise the location and the magnitude of the low-permeability barrier can be still retrieved with an acceptable accuracy.

Experiment No. 3: Low Signal/Noise Ratio. In this experiment we increase the amount of noise in the data. Noise is generated from the same distribution as used in the subsection Experiment No. 3: Parameter Estimation Based on Noisy Measurements: Low Signal/Noise Ratio for the low signal/noise-ratio experiment in the time domain. A Fourier transform is used to transform the noise into the frequency domain. Subsequently, we perform parameter estimation on the basis of this noisy data. The minimization converges in 11 iterations. The truth-, starting-, and estimated-parameter values for this experiment are listed in **Table 7.**

Parameters	Truth Value	Starting Value	Estimated Value
ξ_2	0.7	0.4	0.74
α_b	0.0025	0.75	1.02E–5

Table 7—Model parameters for Experiment No. 3.

It can be interpreted from Tables 6 and 7 that as the noise increases, the accuracy of the estimation of the magnitude parameter becomes worse although the location of the barrier is still accurate. In addition, these results confirm our twin-experiment results in the time domain.

Visualization of the Objective Function

In this section we consider the objective function, expressed in Eq. 36, which is a function of transfer functions S_{11} and S_{12} and we then plot it as a function of our two uncertain parameters (location and magnitude of the barrier) in an attempt to visualize the objective-function shape and its spatial dependence on the two parameters. **Fig. 12** depicts the objective-function surface in the two-variable space. The red dot in Fig. 12 indicates the minimum of the objective function (truth parameters).

If we zoom in on the vicinity of the minimum of Fig. 12, we observe that the surface also displays a varying magnitude with a minimum in the α_b direction **(Fig. 13).**

Figs. 12 and 13 clearly show that our objective function is more sensitive to the barrier location than to the barrier magnitude, which means that, for the currently chosen input/output configuration and input signals, the barrier location has a higher probability to be estimated correctly from noisy data than the permeability magnitude. This behavior was indeed observed in our parameter-estimation results when the amount of noise in the data was increased.

Structural Identifiability

Whether parameters can be uniquely identified from measured data can be considered in two ways. The first approach considers identifiability, or whether through a specific input/output combination we can distinguish a change in any of the parameters (Van Doren 2010). Such an identifiability analysis was performed in the previous sections where we considered a specific input/output configuration with specific inputs and measurement errors. The second approach considers (local) structural identifiability, or whether we can distinguish a change in any of the parameters at all from input/output data, assuming an optimally chosen, "persistently exciting" input. (Glover and Willems 1974; Van den Hof et al. 2009) Such a structural-identifiability analysis is performed in this section by considering the properties of the parameterized-transfer functions, which were derived previously in this study. To this end, we investigate the sensitivity of transfer functions S_{11} and S_{12} with respect to our uncertain parameters (barrier location and barrier magnitude) around the truth parameters. Because the parameters have different orders of magnitude, scaling will influence the identifiable parameter space. Here, we scale the sensitivity vectors by the truth parameters. **Fig. 14** depicts the sensitivity of the system-transfer functions with respect to barrier location and barrier magnitude. It can be clearly seen that the system-transfer functions are more sensitive to the barrier location than to the barrier magnitude for all frequencies considered. This result confirms the findings from the previous sections and, moreover, implies that the difference in

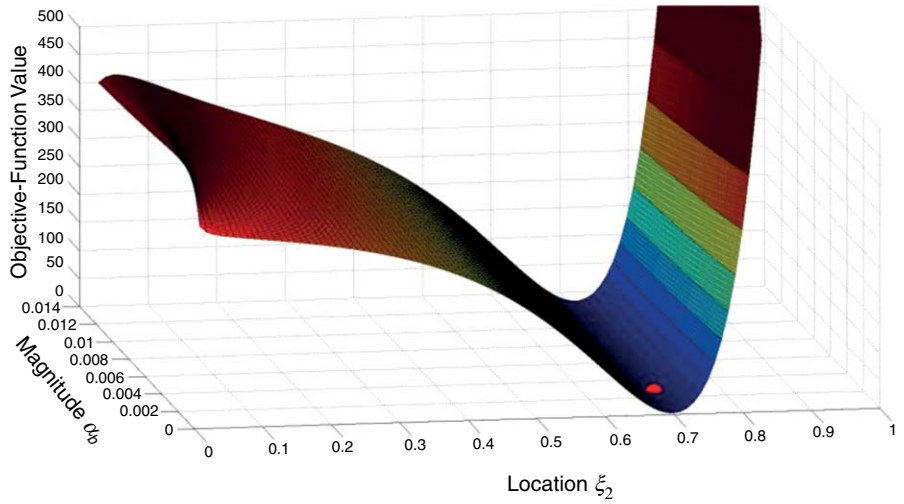

Fig. 12—Objective-function space. The red dot indicates the minimum.

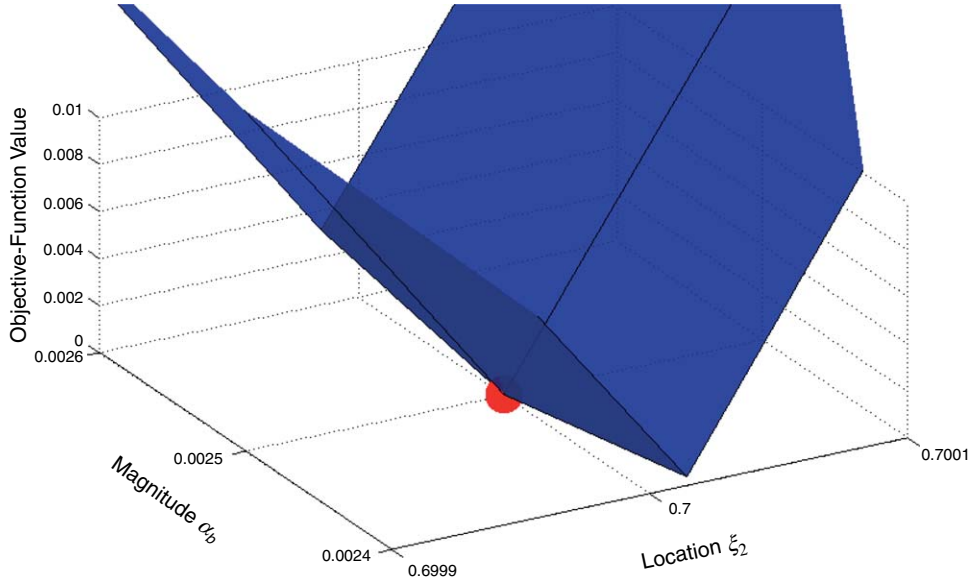

Fig. 13—Zoomed-in objective-function space. The red dot indicates the minimum.

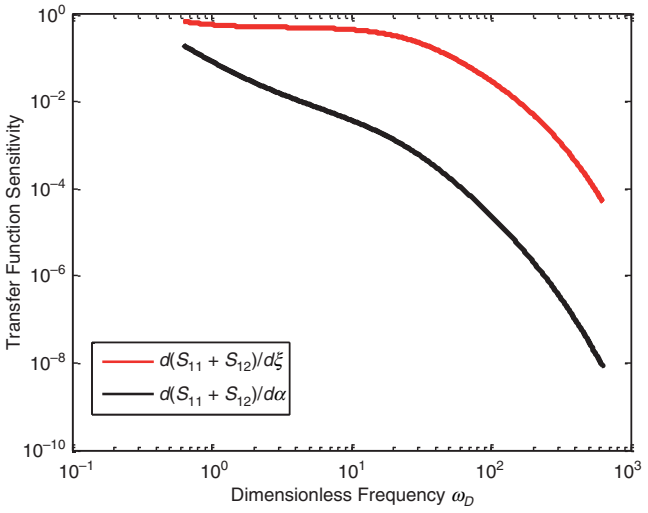

Fig. 14—Sensitivity of transfer functions with respect to barrier location and barrier magnitude.

identifiabilty between location and magnitude is not data-dependent but is a structural property of the system.

Discussion and Conclusions

The time-domain examples presented in this study are derived from experimental results for a model in which only spatially varying permeabilities are parameterized, whereas the frequency-domain examples use a model where a structured physics-based approach is applied in terms of location of the barrier and magnitude of its permeability. We note that there exist techniques to represent the transient response to spatially varying heterogeneities in the Laplace domain with the aid of transformed variables, but we did not pursue these (Levitan and Crawford 2002). In our study the frequency-domain approach therefore uses more prior knowledge (the barrier is parameterized) than the time-domain approach (where all permeabilities are estimated separately). Second, the first approach is truly experiment-driven, whereas the second approach has to the capacity to say something about identifiability independent of the particular experimental data that are used. Moreover, the frequency-domain approach could be used to analyze in which particular frequency region the sensitivity of the parameters is largest, and to design an experiment by picking a

sinusoidal signal of that (maximum sensitive) frequency, for example. Similar ideas have been discussed in the well-testing community since the early 1970s, for purposes of "harmonic testing" (Hollaender et al. 2002).

We note that we could have used the pressure in the injector as an additional output. However, in practice, wellbore pressures in injectors seem to be less frequently available for history-matching studies than wellbore (or tubing-head) pressures in producers. Moreover, pressures in injectors are strongly influenced by the near-wellbore effects of induced fractures, which makes their value for reservoirwide-information inference limited. A similar argument could be made for pressures in the producers, which we used as known inputs, because they may be influenced by the near-wellbore effects of formation damage (skin). We expect that including the injector pressure in our analysis (i.e., adding transfer function S_{21} and S_{22} to Fig. 9) would improve the identifiability, whereas leaving out the producer pressure from the inputs (i.e., removing transfer function S_{12} and only keeping S_{11} in Fig. 9) will deteriorate the identifiability.

In this study, we have investigated the possibility of detecting the location and the magnitude of flow barriers in a 1D reservoir for slightly compressible single-phase flow from the observations (outputs) under different noise conditions. To this end, we have conducted different twin experiments in the time domain and the frequency domain. For the latter, we have developed an analytical expression for the dynamical characteristics of the system as a function of system properties modeled after a transfer-function formalism in the form of bilaterally coupled porous-media models. We conclude the following:

1. The frequency-domain analytical solution makes it possible to investigate the effect of different parameters on the dynamic behavior of the system.
2. It is possible to estimate location and magnitude of a flow barrier from noise-free measurements in slightly compressible single-phase flow.
3. When the noise level in the data is increased, the location of the barrier remains relatively more identifiable than its permeability magnitude.
4. The presence of noise in the data results in unrealistic permeability-magnitude estimates.
5. Visualization of the objective-function space in the frequency domain illustrates that the dynamic output of our system is more sensitive to the barrier location than to barrier magnitude.
6. A structural identifiability analysis by use of the transfer-function approach shows that the difference in identifiability between location and magnitude is not data-dependent but is a structural property of the system.

Nomenclature

A = surface area, L^2, m^2
A_{ij} = transfer functions for block A, dimensionless
B_{ij} = transfer functions for block B, dimensionless
c_t = total compressibility, $Lm^{-1}\,t^2$, Pa^{-1}
C_{ij} = transfer functions for block C, dimensionless
$\mathbf{d}$ = vector of measured data (flow rates), $L^3\,t^{-1}$, m^3/s
J = mismatch objective function in the time domain, dimensionless
k = permeability, L^2, m^2
L = total length of the domain, L, m
$\mathbf{m}$ = vector of unknown model parameters (permeability), L^2, m^2
p = pressure, $L^{-1}m\,t^{-2}$, Pa
$\hat{p}$ = pressure at the outlet boundary, $L^{-1}m\,t^{-2}$, Pa
$\mathbf{P}_d$ = measurement-error correlation matrix, $L^6\,t^{-2}$, m^6/s^2
$\hat{q}$ = flow rate at the inlet boundary, $L^3\,t^{-1}$, m^3/s
s = Laplace variable
S_{ij} = transfer functions for entire system, dimensionless
t = time, t, seconds
V = mismatch objective function in the frequency domain, dimensionless
x = location, L, m
$\mathbf{y}$ = vector of simulated data (flow rates), $L^3\,t^{-1}$, m^3/s
α = dimensionless permeability magnitude
η = hydraulic diffusivity, L^2t^{-1}, m^2/s
θ = dimensionless flow rate
Θ = Laplace-domain dimensionless flow rate
Θ_{obs} = augmented vector of measured data in frequency domain, dimensionless
Θ_{out} = augmented vector of simulated data in frequency domain, dimensionless
μ = viscosity, $L^{-1}m\,t^{-1}$, Pa·s
ξ = dimensionless length
π = dimensionless pressure
Π = Laplace-domain dimensionless pressure
τ = dimensionless time
ϕ = dimensionless porosity
ω_D = dimensionless frequency

Acknowledgments

This research was performed within the context of the Recovery Factory project at Delft University of Technology, sponsored by Shell Global Solutions International. Author M. Mansoori acknowledges the support of D. Rashtchian of the Department of Chemical and Petroleum Engineering of Sharif University of Technology.

References

Ahn, S. and Horne, R. N. 2010. Estimating Permeability Distributions From Pressure Pulse Testing. Presented at the SPE Annual Technical Conference and Exhibition, Florence, Italy, 19–22 September. SPE-134391-PA. http://dx.doi.org/10.2118/134391-MS.

Blom, R. S. and Van den Hof, P. M. 2010. Multivariable Frequency Domain Identification Using IV-based Linear Regression. *Proc.,* 2010 49th IEEE Conference on Decision and Control, Atlanta, Georgia, 15–17 December, 1148–1153. http://dx.doi.org/10.1109/CDC.2010.5717297.

Carslaw, H. S. and Jaeger, J. C. 1959. *Conduction of Heat in Solids*, second edition. Oxford, UK: Oxford University Press.

Dogru, A. H., Dixon, T. N., and Edgar, T. F. 1977. Confidence Limits on the Parameters and Predictions of Slightly Compressible, Single-Phase Reservoirs. *SPE J.* **17** (1) 42–56. SPE-4983-PA. http://dx.doi.org/10.2118/4983-PA.

Feitosa, G. S., Chu, L., Thompson, L. G. et al. 1994: Determination of Permeability Distribution From Well-Test Pressure Data. *J Pet Technol* **46** (7): 607–615. SPE-26047-PA. http://dx.doi.org/10.2118/26047-PA.

Gao, G. and Reynolds, A. C. 2006. An Improved Implementation of the LBFGS Algorithm for Automatic History Matching. *SPE J.* **11** (1) 5–17. SPE-90058-PA. http://dx.doi.org/10.2118/90058-PA.

Glover, K. and Willems, J. C. 1974. Parametrizations of Linear Dynamical Systems: Canonical Forms and Identifiability. *IEEE Trans. Automat. Contr.* **19** (6) 640–646. http://dx.doi.org/10.1109/tac.1974.1100711.

Grader, A. S. and Horne, R. N. 1988. Interference Testing: Detecting a Circular Impermeable or Compressible Subregion. *SPE Form Eval* **3** (2): 420–428. SPE-15585-PA. http://dx.doi.org/10.2118/15585-PA.

Hollaender, F., Hammond, P. S., and Gringarten, A. C. 2002: Harmonic Testing for Continuous Well and Reservoir Monitoring. Presented at the SPE Annual Technical Conference and Exhibition, San Antonio, Texas, 29 September–2 October. SPE-77692-PA. http://dx.doi.org/10.2118/77692-MS.

Joosten, G. J. P., Altintas, A., and Sousa, P. D. 2011. Practical and Operational Use of Assisted History Matching and Model-Based Optimisation in the Salym Field. Presented at the SPE Annual Technical Conference and Exhibition, Denver, 30 October–2 November. SPE-146697-MS. http://dx.doi.org/10.2118/146697-MS.

Kahrobaei, S., Mansoori, M., Joosten, G. J. P. et al. 2014. Hidden Information in Ill-posed Inverse Problems. Oral presentation given at ECMOR XIV – 14th European Conference on the Mathematics of Oil Recovery, Catania, Italy, 8–11 September. http://dx.doi.org/10.3997/2214-4609.20141825.

Kraaijevanger, J. F. B. M., Egberts, P. J. P., Valstar, J. R. et al. 2007. Optimal Waterflood Design Using the Adjoint Method. Presented at the SPE Reservoir Simulation Symposium, Houston, 26–28 February. SPE-105764-MS. http://dx.doi.org/10.2118/105764-MS.

Levitan, M. M. and Crawford, G. E. 2002. General Heterogeneous Radial and Linear Models for Well-Test Analysis. *SPE J.* **7** (2) 131–138. SPE-78598-PA. http://dx.doi.org/10.2118/78598-PA.

Oliver, D. 1996. Multiple Realizations of the Permeability Field From Well Test Data. *SPE J.* **1** (2): 145–154. SPE-27970-PA. http://dx.doi.org/10.2118/27970-PA.

Oliver, D. S., Reynolds, A. C., and Liu, N. 2008. *Inverse Theory for Petroleum Reservoir Characterization and History Matching*. Cambridge, UK: Cambridge University Press.

Shah, P. C., Gavalas, G. R., and Seinfeld, J. H. 1978. Error Analysis in History Matching: The Optimum Level of Parameterization. *SPE J.* **18** (3): 219–228. SPE-6508-PA. http://dx.doi.org/10.2118/6508-PA.

Stallman, R. 1952. *Nonequilibrium Type Curves Modified for Two-Well Systems*. US Department of the Interior.

Van den Hof, P. M., Van Doren, J. F., and Douma, S. G. 2009. Identification of Parameters in Large Scale Physical Model Structures, for the Purpose of Model-Based Operations. In *Model-Based Control – Bridging Rigorous Theory and Advanced Control*, ed. P. M. J. Van den Hof, C. Scherer, and P. S. C. Heuberger, 125–143. New York City: Springer.

Van Doren, J. F. M. 2010. *Model Structure Analysis for Model-Based Operation of Petroleum Reservoirs*. PhD dissertation, Delft University of Technology, Delft, the Netherlands.

Van Doren, J. F. M., Van den Hof, P. M. J., Jansen, J. D. et al. 2008. Determining Identifiable Parameterizations for Large-Scale Physical Models in Reservoir Engineering. *Proc.,* 17th International Federation for Automatic Control World Congress, Seoul, South Korea, 6–11 July, 11421–11426.

Watson, A. T., Gavalas, G. R., and Seinfeld, J. H. 1984. Identifiability of Estimates of Two-Phase Reservoir Properties in History Matching. *SPE J.* **24** (6): 697–706. SPE-12579-PA. http://dx.doi.org/10.2118/12579-PA.

Yaxley, L. M. 1987. Effect of a Partially Communicating Fault on Transient Pressure Behavior. *SPE Form Eval* **2** (4): 590–598. SPE-14311-PA. http://dx.doi.org/10.2118/14311-PA.

Zandvliet, M. J., Van Doren, J. F. M., Bosgra, O. H. et al. 2008. Controllability, Observability and Identifiability in Single-Phase Porous Media Flow. *Computat. Geosci.* **12** (4): 605–622. http://dx.doi.org/10.1007/s10596-008-9100-3.

Siavash Kahrobaei is a PhD degree candidate in the Department of Geoscience and Engineering at Delft University of Technology, in the Netherlands, working on identification of flow-relevant features in history matching. His research interests include data assimilation, reservoir management, and system identification. Kahrobaei holds a bachelor's degree in mining engineering from the University of Tehran, Iran, and a master's degree in petroleum engineering from Delft University of Technology.

Mehdi Mansoori Habibabadi is a PhD degree candidate in the Department of Chemical and Petroleum Engineering at Sharif University of Technology, Iran. He spent 2 years as a guest PhD degree candidate at the Delft University of Technology, in the Netherlands. Mansoori Habibabadi's research interests include pressure-transient analysis and system identification. He holds a master's degree in reservoir engineering and bachelor's degrees in mechanical engineering and reservoir engineering, all from Sharif University of Technology.

Gerard Joosten is a research reservoir engineer at Shell Global Solutions International in Rijswijk, in the Netherlands, currently working on assisted history matching and understanding the physics behind undermodeling. Since he started with Shell in 1994, he has worked on improved oil recovery, predevelopment reservoir-connectivity assessment, well/reservoir interaction, failure modes of electron-gun fabrication, and smart wells and smart fields. Joosten holds a master's degree from Eindhoven University of Technology, in the Netherlands.

Paul Van den Hof is professor of control systems in the Department of Electrical Engineering at Eindhoven University of Technology, in the Netherlands. His current research interests are in system identification and model-based control and optimization, with applications in several technology domains, including petroleum-reservoir-engineering systems. Van den Hof holds master's and PhD degrees from Eindhoven University of Technology.

Jan-Dirk Jansen is professor of reservoir systems and control and head of the Department of Geoscience and Engineering at Delft University of Technology, in the Netherlands. Previously, he worked for Shell International in research and operations. Jansen's current research interests are the use of systems and control theory for production optimization and reservoir management. He holds master's and PhD degrees from Delft University of Technology.